Journal of Energetic Materials
Publication details, including instructions for authors and subscription information:
http://www.informaworld.com/smpp/title~content=t713770432

Quantum Chemistry-Based Force Field for Simulations of Energetic Dinitro Compounds

Hemali Davande[a]; Oleg Borodin[a]; Grant D. Smith[a]; Thomas D. Sewell[b]
[a] Department of Chemical Engineering and Department of Materials Science & Engineering, University of Utah, Salt Lake City, UT, USA [b] Theoretical Division, Los Alamos National Laboratory, Los Alamos, NM, USA

To cite this Article Davande, Hemali , Borodin, Oleg , Smith, Grant D. and Sewell, Thomas D.(2005) 'Quantum Chemistry-Based Force Field for Simulations of Energetic Dinitro Compounds', Journal of Energetic Materials, 23: 4, 205 — 237
To link to this Article: DOI: 10.1080/07370650591006885
URL: http://dx.doi.org/10.1080/07370650591006885

Energetic Materials, 23: 205–237, 2005

ISSN: 0737-0652 print
DOI: 10.1080/07370650591006885

Taylor & Francis
Taylor & Francis Group

Quantum Chemistry–Based Force Field for Simulations of Energetic Dinitro Compounds

HEMALI DAVANDE
OLEG BORODIN
GRANT D. SMITH

Department of Chemical Engineering and Department of Materials Science & Engineering, University of Utah, Salt Lake City, UT, USA

THOMAS D. SEWELL

Theoretical Division, Los Alamos National Laboratory, Los Alamos, NM, USA

A quantum chemistry–based force field for molecular dynamics simulations of energetic dinitro compounds has been developed, based on intermolecular binding energies, molecular geometries, molecular electrostatic potentials, and conformational energies obtained from quantum chemistry calculations on model compounds. Nonbonded parameters were determined by fitting experimental densities and heats of vaporizations of model compounds. Torsional parameters were parameterized to reproduce accurately the relative conformational energy minima and barriers in 2,2-dinitropropane, di-methoxy di-methyl ether, 2,2-dinitro-3-methoxypropane, and bis(2,2-dinitropropyl)formal. Molecular dynamics simulations using the developed force field accurately reproduce thermodynamic and transport properties of 1,1-dinitroethane,

Address correspondence to G. D. Smith, Department of Chemical Engineering and Department of Materials Science & Engineering, 122 South Central Campus Dr., Room 304, University of Utah, Salt Lake City, Utah, 84112, USA. E-mail: hemali.davande@utah.edu

2,2-dinitropropane, and a eutectic mixture of bis(2,2-dinitropropyl)formal and bis(2,2-dinitropropyl)acetal.

Keywords: PBX, molecular orbital calculations, heterogeneous explosives

1. Introduction

Dinitro compounds have important applications as components of rocket propellant charges and as plasticizers in plastic-bonded explosives (PBXs), due in part to their relatively large decomposition energies [1]. We are interested in using molecular simulations to improve our understanding of the mechanical and thermophysical behavior of PBXs, in particular PBX-9501 [2], which is composed of 94.9-wt% HMX (octahydro-1,3,5,7-tetranitro-1,3,5,7-tetrazocine), 2.5-wt% Estane^{TM} 5703 [poly(butylene adipate-co-tetramethylene diphenyl-urethane), hereafter referred to simply as Estane], and 2.5-wt% nitroplasticizer [50/50-wt% eutectic of bis(2,2-dinitropropyl) formal/acetal, denoted hereafter as BDNPF/A]. Molecular modeling of PBX-9501 composites and specific interactions among its components has been complicated by the absence of accurate force fields for the constituent materials. This paper is one in a series of reports on force field development and molecular simulations of PBX-9501 constituents. Force field development and validation for HMX [3] and Estane [4] has been reported previously; analogous development and validation of a quantum chemistry–based force field for model dinitro compounds and dinitro plasticizer are reported here.

BDNPF/A plasticizer is cost effective to use and safe to handle. It provides excellent propellant and explosive physical properties and enhances the performance of formulations while providing additional energy to the composite. It also exhibits good long-term stability. BDNPF/A plasticizer acts as a lubricant within the polymeric binder network, reducing the elastic modulus and lowering the glass transition temperature of the polymer. Large amounts of energetic plasticizer can increase the specific impulse of the propellant and reduce the possibility

of cracking [5]. BDNPF/A is used in both U.S. and British systems, for example, U.S. Navy underwater and airburst plastic-bonded explosive formulations [6]. It is widely used in warheads for torpedoes, missiles, and projectiles. Most recent applications of this material have been in low-vulnerability gun propellant, insensitive high explosives, and insensitive munitions, all used and currently fielded by the U.S. Army [6]. Plasticized polyurethanes are used as binders for high explosives to impart structural integrity to the composite, aid in processing, and decrease the sensitivity to external stimuli [7]. Although both BDNPF and BDNPA are solid at room temperature, the 50/50-wt% mixture of the two forms a eutectic with a lower melting point than early plasticizers such as nitroglycerin and diethyl phthalate [8].

Atomistic classical molecular dynamics (MD) simulations can provide molecular-level understanding of the partitioning of nitroplasticizer between the ''hard'' and ''soft'' segment-rich domains [4] in microphase-segregated, segmented poly(ester urethane), the resulting domain structure; and the influence of this domain structure, on thermodynamic, mechanical, dynamic, and transport properties of the binder. To utilize atomistic MD simulations for studies of PBX-9501 binder, accurate descriptions of the molecular geometry and conformational energetics of Estane and BDNPF/A nitroplasticizer are required. The formulation of a quantum chemistry–based force field for BDNPF is the principal subject of the present work.

We report in Section 2 high level *ab initio* quantum chemistry calculations for some important energetic dinitro compounds, including BDNPF, 2,2-dinitro-3-methoxypropane (DNMP), and di-methoxy di-methyl ether (DMDME). In Section 3, a classical, analytic force field is developed based on fitting the equilibrium geometries and conformational energetics obtained from the quantum chemistry calculations described in Section 2, with subsequent minor adjustments to match the available thermodynamic data. The ability of the resultant force field to reproduce accurately thermodynamic and transport properties of dinitro compounds is presented and discussed in Section 4.

2. Quantum Chemistry Calculations

In this section we report *ab initio* quantum chemistry calculations of equilibrium geometries and conformational energetics of several compounds that will be utilized in the actual force field parameterization for BDNPF. As we cannot perform extensive high-level quantum chemistry studies on the full BDNPF molecule (Figure 1(a)) or BDNPA molecule (Figure 1(b)), we carried out most of our investigations for smaller dinitro compounds that possess subsets of the chemical linkages and dihedral arrangements that occur in BDNPF (Figures 1(c)–1(e)). However, the combined set of model compounds spans the set of relevant interactions in BDNPF. We performed quantum chemistry calculations only for the full BDNPF molecule for a selection of low-energy conformations as a test of transferability of the force field developed on the basis of the smaller compounds to the target molecule.

All *ab initio* quantum chemistry calculations were performed using the Gaussian 98 package [9]. Density functional and Hartree-Fock theory were used for initial geometry optimizations of the model compounds. The hybrid B3LYP functional [10,11] and 6-31G* basis sets were used for DNP, DNMP, DMDME, and BDNPF. Following our previous work on a variety of polymers including polyethylene oxide, polypropylene oxide, 1,2-dimethoxyethane [12,13], HMX [3], and Estane [4], we used these comparatively inexpensive ''scoping'' calculations as a starting point for determination of more accurate conformational geometries and energetics at the B3LYP, HF, and MP2 levels, using the B3LYP/aug-augmented correlation consistent polarized valence double-ζ basis sets (aug-cc-pvDz) [14].

Conformational energies and geometries for DMDME, DNP, and DNMP for important conformers and rotational barriers corresponding to HF, B3LYP, and MP2 theory in conjunction with the aug-cc-pvDz basis set are summarized in Tables 1–3, respectively, and will be discussed in subsequent sections.

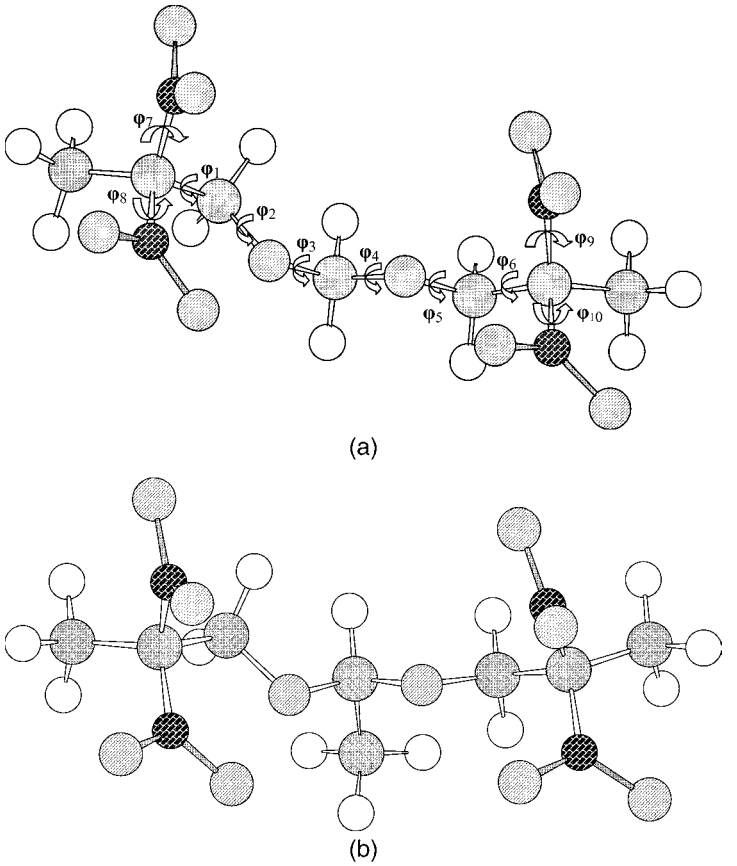

Figure 1. Molecular structures. *Circles with brick pattern*: nitrogen; *empty circles*: hydrogen; *gray circles*: carbon; *circles with diagonal hash*: oxygen. (a) Labeling of the unique torsions in bis(2,2-dinitropropyl)formal (BDNPF). $\varphi_{\mathbf{1}}$ and $\varphi_{\mathbf{6}}$ are C−C−C−O torsions; $\varphi_{\mathbf{3}}$ and $\varphi_{\mathbf{4}}$ are C−O−C−O torsions; $\varphi_{\mathbf{5}}$ and $\varphi_{\mathbf{2}}$ are C−O−C−C torsions; and $\varphi_{\mathbf{7}}$, $\varphi_{\mathbf{8}}$, $\varphi_{\mathbf{9}}$ and $\varphi_{\mathbf{10}}$ are O−N−C−C torsions. (b) bis(2,2-dinitropropyl)acetal (BDNPA). (c) di-methoxy di-methyl ether (DMDME). $\varphi_{\mathbf{11}}$ and $\varphi_{\mathbf{12}}$ are C−O−C−O torsions. (d) 2,2-dinitro-3-methoxy propane (DNMP). (e) 2,2-dinitropropane (DNP).

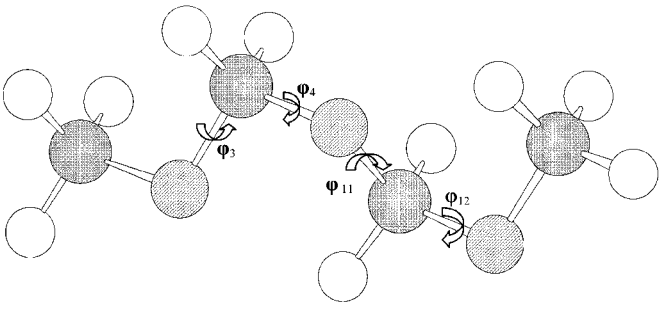

(c)

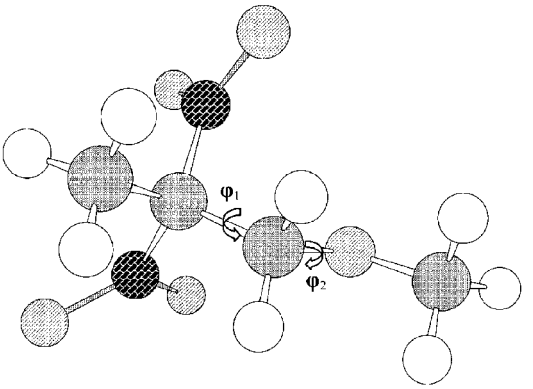

(d)

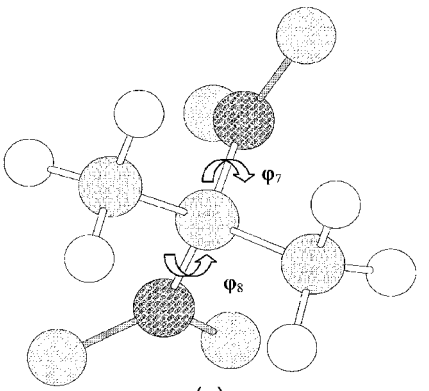

(e)

Figure 1. Continued.

Table 1
Relative conformational energies for di-methoxy di-methyl ether (DMDME) as obtained from the parameterized force field (normal text) and quantum chemistry (MP2/aug-cc-pvDz//B3LYP/aug-cc-pvDz, italics)

		Torsional angles (degree)			
Conformer	Energy (kcal/mol)	$\boldsymbol{\varphi_3}$[a]	$\boldsymbol{\varphi_4}$	$\boldsymbol{\varphi_{11}}$	$\boldsymbol{\varphi_{12}}$
gggg	0.00	78.0	83.7	83.7	78.1
	0.00	*68.2*	*73.4*	*74.3*	*68.7*
gg145g[b]	3.95	79.0	80.3	**145.0**[c]	79.0
	3.11	*68.7*	*70.5*	***145.0***	*69.0*
gg152g	3.31	78.9	81.4	**152.0**	79.3
	3.05	*68.7*	*69.9*	***152.0***	*69.0*
ggtg	1.11	79.7	85.1	182.2	79.5
	2.98	*68.7*	*70.5*	*159.7*	*69.0*
gg220g	3.42	80.9	84.7	**220.9**	80.4
	3.10	*73.7*	*79.1*	***220.9***	*73.5*
ggg$^-$*g*	1.53	75.4	91.3	272.5	94.5
	2.83	*66.0*	*87.0*	*265.0*	*85.0*
gg345g	9.31	75.0	76.9	**345.0**	100.5
	9.09	*65.6*	*88.3*	***345.0***	*103.6*
ggg$^-$*g*$^-$	1.36	78.7	83.0	276.9	281.2
	1.66	*71.6*	*97.0*	*296.0*	*294.5*
g138g$^-$*g*$^-$	3.66	79.6	**138.0**	279.9	284.2
	3.15	*60.0*	***138.0***	*293.0*	*294.0*
g$^-$*tg*$^-$*g*$^-$	1.11	280.5	177.8	274.8	280.4
	2.42	*292.0*	*196.0*	*291.0*	*292.0*

[a] $\boldsymbol{\varphi_3}$, $\boldsymbol{\varphi_4}$, $\boldsymbol{\varphi_{11}}$, and $\boldsymbol{\varphi_{12}}$ are the C−O−C−O torsions in DMDME (see Figure 1(c)).

[b] The conformer notation *gg145g* means torsion $\boldsymbol{\varphi_{11}}$ was constrained to 145°.

[c] Numbers in bold denote constrained torsions.

Table 2
Relative conformational energies for 2,2-dinitropropane (DNP) as obtained from the parameterized force field (normal text) and from quantum chemistry (MP2/aug-cc-pvDz//B3LYP/aug-cc-pvDz, italics)

Conformer	Energy (kcal/mol)	Torsion $\boldsymbol{\varphi_7}$[a] (degree)	Torsion $\boldsymbol{\varphi_8}$ (degree)
tg^+	0.00	161.6	96.0
	0.00	*167.4*	*111.1*
*180*g^+[b]	0.40	**180.0**[c]	90.1
	0.31	***180.0***	*102.9*
*150*g^+	0.27	**150.0**	101.1
	0.38	***150.0***	*121.5*
*135*$t\_$	0.99	**135.0**	143.8
	0.98	***135.0***	*133.2*
*120*$t\_$	1.23	**120.0**	152.4
	1.35	***120.0***	*150.3*
*105*t	1.00	**105.0**	160.4
	1.14	***105.0***	*167.6*
*90*t	0.32	**90.0**	193.2
	0.59	***90.0***	*179.3*
*75*t	0.01	**75.0**	199.1
	0.09	***75.0***	*188.0*
g^+t	0.32	**90.0**	**180.0**
	0.58	***90.0***	***180.0***
$g^+t\_$	1.24	**120.0**	**150.0**
	1.36	***120.0***	***150.0***
$g^+t\_$(saddle)[d]	1.22	**117.6**	**153.7**
	1.38	*117.6*	*153.4*
$gt\_$(saddle)	1.81	**26.6**	**154.1**
	2.63	*26.6*	*154.1*
$g^+g\_$	1.23	**120.0**	**330.0**
	1.36	***120.0***	***330.0***

(*Continued*)

Table 2
Continued

Conformer	Energy (kcal/mol)	Torsion $\boldsymbol{\varphi_7}$[a] (degree)	Torsion $\boldsymbol{\varphi_8}$ (degree)
g^+ *cis*	1.96	**120.0**	**0.0**
	2.39	***120.0***	***0.0***

[a] $\boldsymbol{\varphi_7}$ and $\boldsymbol{\varphi_8}$ represent O−N−C−C torsions in DNP (see Figure 1(e)).

[b] The conformer *180*g^+ means torsion $\boldsymbol{\varphi_7}$ was constrained to 180°.

[c] Numbers in bold font denote constrained torsions.

[d] The ''saddle'' notation here corresponds to single-point calculations done using quantum chemistry studies. The corresponding molecular mechanics energies were obtained by constraining the torsions $\boldsymbol{\varphi_7}$ and $\boldsymbol{\varphi_8}$ to quantum chemistry values.

Table 3
Relative conformational energies for 2,2-dinitro-3-methoxy propane (DNMP) as obtained from the parameterized force field (normal text) and from quantum chemistry (MP2/aug-cc-pvDz//B3LYP/aug-cc-pvDz, italics)

Conformer	Energy (kcal/mol)	Torsion $\boldsymbol{\varphi_1}$[a] (degree)	Torsion $\boldsymbol{\varphi_2}$ (degree)
gt	0.00	62.3	172.3
	0.00	*62.3*	*175.3*
tt	2.55	182.8	178.0
	2.67	*167.0*	*176.0*
tg	3.07	162.7	74.9
	3.85	*156.0*	*88.8*
gg	2.95	**60.0**[b]	**60.0**
	3.31	***60.0***[b]	***60.0***

(*Continued*)

Table 3
Continued

Conformer	Energy (kcal/mol)	Torsion $\boldsymbol{\varphi_1}$[a] (degree)	Torsion $\boldsymbol{\varphi_2}$ (degree)
g95[c]	1.56	54.9	**95.0**
	1.18	*55.0*	***95.0***
gg^-	4.46	**60.0**	**280.0**
	4.44	***60.0***	***280.0***
gg^- (saddle)[d]	2.95	82.5	277.5
	3.39	*82.5*	*277.5*
tg^+	3.07	162.7	75.0
	3.69	*160.6*	*110.4*
120t	6.47	**120.3**	156.0
	6.68	***120.3***	*176.5*
g120	0.90	66.3	**120.0**
	0.92	*63.1*	***120.0***
cisg	5.41	**0**	**97.9**
	5.55	***0.50***	***97.9***
cisg (saddle)	5.51	351.7	101.4
	5.67	*351.7*	*101.4*
cist	4.57	**0**	181.5
	4.47	***0***	*183.4*
cist (saddle)	4.66	**6.1**	**180.9**
	4.63	*6.1*	*180.9*

[a] $\boldsymbol{\varphi_1}$ and $\boldsymbol{\varphi_2}$ represent C−C−C−O and C−O−C−C torsions, respectively (see Figure 1(d)).

[b] Bold font is used to identify the constrained torsions.

[c] The conformer notation *g95* means torsion $\boldsymbol{\varphi_2}$ was constrained to 95°.

[d] The "saddle" notation here corresponds to single-point calculations done using quantum chemistry studies. The corresponding molecular mechanics energies were obtained by constraining the torsions $\boldsymbol{\varphi_1}$ and $\boldsymbol{\varphi_2}$ to quantum chemistry values.

3. Force Field Development

Methodology

The classical force field represents the total potential energy $V(r)$ of a collection of atoms with positions given by the vector $\vec{R}$ as a sum of nonbonded interactions $V^{NB}(\vec{R})$ and energy contributions due to all bond, valence bend, torsional, and deformational interactions:

$$V(\vec{R}) = V^{NB}(\vec{R}_{ij}) + \sum_{bonds} V^{BOND}(r_{ij}) + \sum_{bends} V^{BEND}(\theta_{ijk}) + \sum_{torsions} V^{TORS}(\varphi_{ijkl}) + \sum_{deformations} V^{DEFORM}(\delta_{ijkl}). \quad (1)$$

The nonbonded energy $V^{NB}(\vec{R}_{ij})$ consists of a sum of the two-body repulsion and dispersion energy terms between atoms i and j, represented by the Buckingham exponential-6 potential, and the energy due to the interactions between fixed partial atomic charges (i.e., Coulombic terms):

$$V^{NB}(\vec{R}_{ij}) = \frac{1}{2}\sum_{i,j=1}^{N} A_{ij}\exp(-B_{ij}R_{ij}) - \frac{C_{ij}}{R_{ij}^6} + \frac{q_i q_j}{4\pi\varepsilon_o R_{ij}}. \quad (2)$$

Nonbonded interactions were included between all atoms of different molecules and between atoms of the same molecule separated by more than two bonds (1–4 interactions included). The following combining rules were used to evaluate interactions between different types of atoms:

$$\begin{aligned} A_{ij} &= \sqrt{A_{ii}A_{jj}}, \\ B_{ij} &= \frac{B_{ii} + B_{jj}}{2}, \\ C_{ij} &= \sqrt{C_{ii}C_{jj}}. \end{aligned} \quad (3)$$

Contributions due to covalent interactions were represented as the following:

$$V^{BOND} = \frac{1}{2}k_{ij}^{bond}(r_{ij} - r_{ij}^0)^2, \quad (4)$$

$$V^{BEND}(\theta_{ijk}) = \frac{1}{2} k_{ijk}^{bend} (\theta_{ijk} - \theta_{ijk}^0)^2, \tag{5}$$

$$V^{TORS}(\varphi_{ijkl}) = \frac{1}{2} \sum_n k_{ijkl}^{tors}(n)[1 - \cos(n\varphi_{ijkl})], \tag{6}$$

$$V^{DEFORM} = \frac{1}{2} k_{ijkl}^{d} \delta_{ijkl}^2. \tag{7}$$

Here r_{ij}^0 is an equilibrium bond length,[1] θ_{ijk}^0 is an equilibrium valence bend angle, and δ_{ijkl} is an out-of-plane bend (i.e., the angle between the plane containing atoms i, j, and k and the bond between atoms k and l); k_{ij}^{bond}, k_{ijk}^{bend}, k_{ijkl}^{tors} (n), and k_{ijkl}^{d} are the bond, bend, torsion, and deformation force constants, respectively. The indices indicate which (bonded) atoms are involved in the interaction.

In this contribution we follow the force field development methodology applied previously to HMX [3], Estane [4], and a number of other polymers [12,13]. Specifically, we obtain partial atomic charges by fitting the electrostatic potential obtained from a quantum mechanical wavefunction/density on a grid of points for each of the model compounds. We either use published repulsion/dispersion parameters for compounds with chemical environments similar to those of interest here, or fit them ourselves to available thermodynamic data for those compounds for which interaction parameters have not been reported. The ''equilibrium'' bond lengths and bending angles are adjusted to reproduce equilibrium geometries of model compounds obtained from quantum chemistry. Finally, we fit the torsional parameters to reproduce the geometries and conformational energetics of model compounds, obtained from high-level quantum chemistry calculations.

[1]Note that the natural bond length or bond angle for a given bond or valence angle does not necessarily correspond to the bond length or angle of the molecular mechanics optimized geometry of a molecule. Nonbonded interactions can result in an optimized bond length or angle that differs from the equilibrium value.

Repulsion/Dispersion Parameters

The parameters for carbon (C) and hydrogen (H) were taken from our previous studies on polyethylene and poly(oxymethylene) [15]. It was found that the repulsion/dispersion parameters for nitrogen and oxygen taken from studies on HMX [3], where they were derived for a nitro ($-NO_2$) group attached to nitrogen, were not suitable to describe the potential energy and the dynamics for compounds containing the dinitro functionality attached to carbon. Thus, using the calculated charges and optimized geometric parameters, the repulsion/dispersion parameters for nitrogen and oxygen were adjusted to yield the best overall agreement between experimental densities and enthalpies of vaporization and those calculated from liquid phase molecular dynamics (see Table 4), for DNP, DNE, BDNPF, and BDNPF/A. Once this initial set of ''optimal'' nonbonded parameters was obtained, the entire procedure, starting from refits of the valence parameters, was reiterated multiple times until a converged best fit was obtained. The resulting optimized repulsion/dispersion parameters are reported in Table 5.

Partial Atomic Charges

The different atom types employed for determination of partial charges are illustrated in Figure 2. The different charge groups used were (1) C_e, for carbon atoms in end groups (CH_3) of BDNPF; (2) C_n, for carbon atoms attached to NO_2 groups; (3) C_n, for carbon atoms attached to oxygen (atom of type O, see below) on one side and carbon atom of type C_n on the other side; (4) C_l, for carbon atoms attached to carbon atoms of type C_n and C_e in DNMP; (5) C_{ll}, for carbon atoms attached to oxygen atoms (of type O, see below) on both sides of the central carbon in BDNPF; (6) O, for oxygen; (7) O_n, for oxygen atoms in an NO_2 group; (8) H, for hydrogen atoms attached to carbon atom of type C_e; (9) H_m, for hydrogen atoms attached to carbon atoms of type C_n; and (10) H_l, for hydrogen atoms attached to carbon atoms of type C_l (in DNMP) or C_{ll} (in BDNPF). We

Table 4
Comparison of thermodynamic properties obtained from simulations to experimental results (in parentheses)

Liquid	Temperature (K)	Box size (Å)	Rouse time (ps)	Equilibration time (ns)	Production run time (ns)	Density (g/cc)	Enthalpy of vaporization (kcal/mol)
DNP[a]	298	25.9	20	1.0	NPT-1.5	1.267	13.8
					NVT-1.5	(1.3)[b]	(13.7)[c]
DNE[d]	298	24.7	15	1.0	NPT-2.0	1.316	14.2
					NVT-2.0	(1.354)[e]	(14.6)[c]
BDNPF[f]	400	22.3	600	3.0	NPT-3.0	(—)[g]	22.6
					NVT-2.0		(17.9)[h]
Eutectic mixture	298	29.0	30,000	5.0	NPT-8.0	1.359 (1.383–1.397)[i]	(—)[g]

[a] 2,2-dinitropropane, see Figure 1(e).
[b] Reference [**25**].
[c] Reference [**24**].
[d] 1,1-dinitroethane.
[e] Reference [**23**].
[f] bis(2,2-dinitropropyl)formal, see Figure 1(a).
[g] No experimental results are available for comparison.
[h] Reference [**26**] and see text in Section 4.
[i] Reference [**26**].

Table 5
Final repulsion (A and B) and dispersion (C) force field parameters

Nonbonded, $U^{NB}\vec{R} = \frac{1}{2}\sum_{i,j=1}^{N} A_{ij}\exp(-B_{ij}R_{ij}) - \frac{C_{ij}}{R_{ij}^6}$				
Atom pair	A_{ij} (kcal/mol)	B_{ij}(Å^{-1})	C_{ij} (kcal mol^{-1} Å^{-6})	Source
C−C	14976.00	3.09	640.08	[15]
O−O	78877.76	4.06	319.12	This work
N−N	63267.40	3.78	250.00	This work
H−H	2649.60	3.74	27.40	[15]
C−H	4320.00	3.42	138.24	[15]

used MP2/aug-cc-pvDz//B3LYP/aug-cc-pvDz for determination of charges, for the lowest energy conformations obtained for each model compound. Note that new atom types were defined for hydrogen atoms bonded to carbons, which are bonded in turn to comparatively electronegative atoms. The standard electrostatic potential (ESP) derived charges are the coefficients that yield the optimal least-squares fit to the model function for the given set of ESP points.

Within this approach, charges obtained for the internal atoms can fluctuate significantly, while exerting only minimal influence on the objective function (χ^2) for the fit to the ESP. To mitigate this effect, the partial atomic charges for the model compounds and BDNPF were determined using restrained electrostatic potential (RESP) fitting [16,17]. The electrostatic potential envelope cutoffs were set to the van der Waals radii: 1.8 Å for hydrogen, 2.5 Å for carbon and nitrogen, and 2.0 Å for oxygen. The electrostatic potential was evaluated at approximately 350,000 points for each model compound; the fit was constrained to yield net charge neutrality for each molecule. The partial atomic charges for different atom types in DNMP, DNP, and BDNPF are given in Table 6.

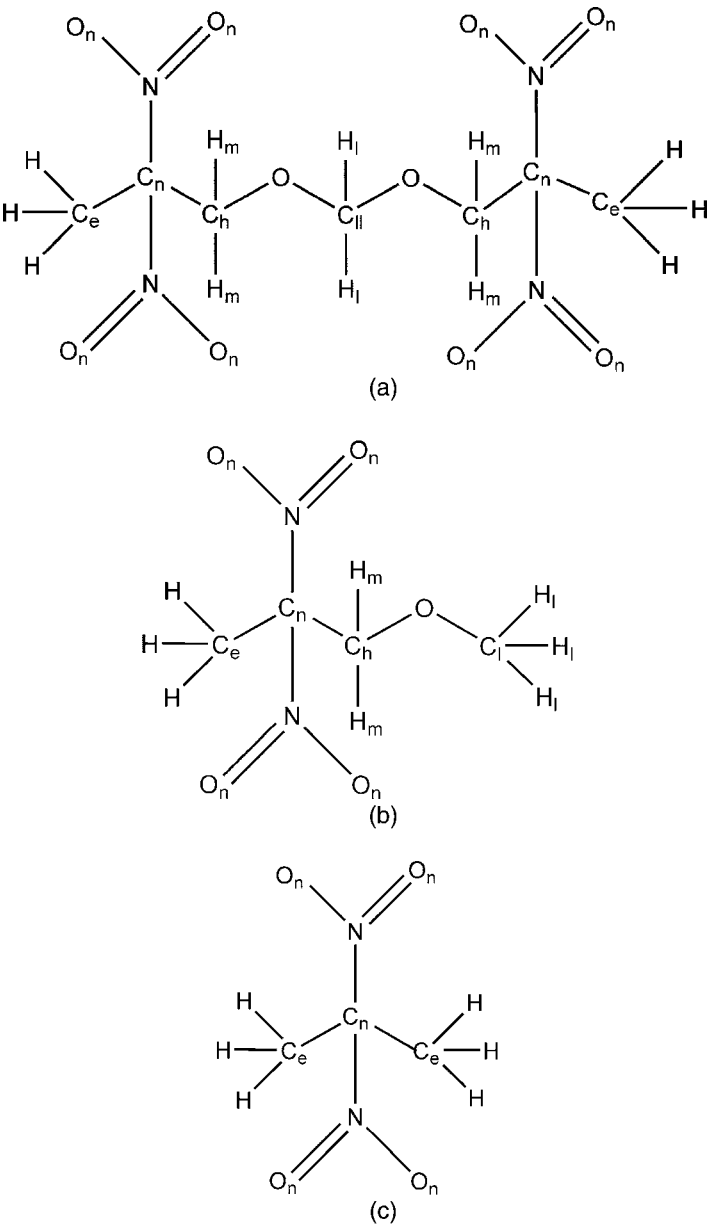

Figure 2. Atom type definitions for assigning partial atomic charges in (a) bis(2,2-dinitropropyl)formal (BDNPF), (b) 2,2-dinitro-3-methoxy propane (DNMP), (c) 2,2-dinitropropane (DNP).

Table 6
Partial atomic charges for model compounds and BDNPF, calculated using quantum chemistry (MP2/aug-cc-pvDz// B3LYP/aug-cc-pvDZ)

Atom type	DNMP[a]	DNP[b]	BDNPF[c]
C_e^d	–0.1809	–0.6079	–0.1809
C_n	0.2855	0.5646	0.2855
C_h	–0.1314	–	–0.1314
N	0.5122	0.5178	0.5122
O	–0.2364	–0.3708	–0.2364
O_n	–0.3444	–	–0.3444
H	0.0825	0.1831	0.0825
C_l	–0.2024	–	–
H_m	0.1035	–	0.1035
H_l	0.1221	–	0.1221
C_{ll}	–	–	0.0835

[a] 2,2-dinitro-3-methoxy propane (see Figure 1(d)).
[b] 2,2-dinitropropane (Figure 1(e)).
[c] bis(2,2-dinitroproyl)formal (Figure 1(a)).
[d] Refer to Figure 2 for atom type definitions.

Bonded Interaction Parameters

The values for k^{bond} and k^{bend} were taken from work on HMX [3], Estane [4], polyethylene and poly(oxymethylene) [15], and poly(oxyethylene) and 1,2-dimethoxyethane [18]. Molecular mechanics geometry optimization was performed on each model compound, with initial guesses for equilibrium bond lengths r_0 and bond angles θ_0. The values of bond lengths r_0 and bond angles θ_0 (taken from the corresponding references for k^{bond} and k^{bend}) were adjusted to provide the best match between molecular mechanics– and quantum chemistry–optimized geometries. The results are listed in Table 7. In the final pass for optimization of r_0 and θ_0, the repulsion/dispersion parameters given in Table 4 and the partial charges given in Table 6 were used. The optimized r_0 and θ_0 from DNMP were used for

Table 7
Bis(2,2-dinitropropyl)formal (BDNPF) force field (covalent interactions only)

$V^{bond}(r_{ij}) = \frac{1}{2}k_{ij}^{bond}(r_{ij} - r_{ij}^{0})^2$					
Bond type	k^{bond} (kcal mol^{-1} Å^{-2})	r_0 (Å)	QC (Å) (avg)	MM (Å) (avg)	Source
C–C	618.0	1.468	1.522	1.498	[15]
C–H	655.0	1.098	1.098	1.087	[15]
C–N	672.0	1.512	1.545	1.526	[4]
O–N	1990.1	1.221	1.220	1.222	[3]
C–O	739.0	1.406	1.418	1.412	[15]

$V^{bend}(\theta_{ijk}) = \frac{1}{2}k_{ijk}^{bend}(\theta_{ijk} - \theta_{ijk}^{0})^2$					
Bend type	k^{bend} (kcal mol^{-1} rad^{-2})	θ_0 (degree)	QC (degree)[a]	MM (degree)[b]	Source
C–C–C	105.0	122.1	114.9	114.9	[15]
C–C–O	119.0	104.9	106.5	106.8	[18]

C–O–C	149.0	111.2	112.6	113.5	[15]
C–C–H	85.80	110.10	109.9	110.5	[15]
C–C–N	144.0	109.4	109.3	108.2	[4]
O–N–C[c]	125.0	112.9	116.8	116.6	[3]
H–C–O	112.0	107.1	109.6	108.9	[15]
H–C–H	77.0	108.5	109.5	108.2	[15]
O–N–O	125.0	126.4	126.5	126.5	[3]
N–C–N	144.0	116.2	104.0	109.0	[3]
O–C–O	144.0	120.8	–	–	[4]

$V^{tors}(\phi_{ijkl}) = \sum_n \frac{1}{2} k_{ijkl}^{tors}(n)[1 - \cos(n\phi_{ijkl})]$

Torsion	k_1^{tors} (kcal/mol)	k_2^{tors} (kcal/mol)	k_3^{tors} (kcal/mol)	k_4^{tors} (kcal/mol)	Source
C–C–C–O	–1.8990	0.6950	2.7000	–	This work
C–C–O–C	5.8950	1.4594	0.0005	–	This work
H–C–C–C	0.0000	0.0000	−0.2779	–	[15]
O–N–C–C	3.5000	0.0000	–2.5997	–	This work
N–C–C–O	–3.1250	1.1150	–1.1900	–	This work
H–C–O–C	0.0000	0.0000	−0.7290	–	[15]

(*Continued*)

Table 7
Continued

$V^{tors}(\phi_{ijkl}) = \sum_n \frac{1}{2} k^{tors}_{ijkl}(n)[1 - \cos(n\phi_{ijkl})]$					
Torsion	k^{tors}_1 (kcal/mol)	k^{tors}_2 (kcal/mol)	k^{tors}_3 (kcal/mol)	k^{tors}_4 (kcal/mol)	Source
H−C−C−N	0.0000	0.0000	−0.2779	–	Same as −HCCC
O−N−C−N	0.0000	0.0000	0.0000	–	–
C−O−C−O	−0.5948	–2.1934	−0.1790	1.9800	This work

$V^{deform} = \frac{1}{2} k^d_{ijkl} \delta^2_{ijkl}$		
Out-of-plane bend	k^{d} (kcal mol^{-1} rad^{-2})	Source
O−N−O−C[d]	89.3	[3]

[a] Optimized geometry obtained at MP2/aug-cc-pvDz//B3LYP/aug-cc-pvDZ level of quantum chemistry.
[b] Optimized geometry obtained using molecular mechanics minimization of the BDNPF force field.
[c] The force constant for the O−N−O bend is assumed equal to that for the O−N−C bend.
[d] Taken from the out-of-plane bend constant for O−N−O−N derived for HMX [3].

BDNPF. The mean-square error for all bonds was 0.009 Å, and that for the valence bends was 1.9°. These small fiducials suggest good transferability of the force field developed from smaller model compounds to BDNPF/A system.

Torsional Parameters

Because the expense of sufficiently high-level quantum chemistry calculations precludes us from accurate determination of all BDNPF conformers and barriers among them, we have chosen to fit torsional parameters for representative model compounds and check their transferability to BDNPF by comparing molecular mechanics and quantum chemistry results only for the most important conformers in BDNPF. The torsional parameters were optimized for model compounds, using optimized bond lengths and bond angles from Table 7, partial atomic charges from Table 6 (DNMP), and nonbonded parameters from Table 5.

The torsional parameters for C−O−C−O were obtained from the molecular mechanics force field for DMDME (Figure 1(c)). To achieve direct transferability of the torsional parameters, the charges on the atoms for DMDME were taken from BDNPF. A comparison of energies and geometries of DMDME from quantum chemistry and the force field is given in Table 1.

For DNP the parameters for the O−N−C−C torsion (Figure 1(e)) were adjusted to yield the best agreement between the conformational energies and geometries obtained from quantum chemistry (MP2/aug-cc-pvDz//B3LYP/aug-cc-pvDz) and molecular mechanics. From the conformational energy plot for DNP shown in Figure 3, we conclude that the molecular mechanics force field accurately reproduces the saddle points and minima for this model compound. The minimum energy O−N−C−C (φ_7,φ_8) conformation at the MP2/aug-cc-pvDz//B3LYP/aug-cc-pvDz level was found to be tg^+ (161.6°, 96.0°), and the maximum-energy conformation was found to be *gt-saddle* (26.6°, 154.1°) with an energy 2.63 kcal/mol relative to the minimum energy conformation. The energies of all the conformations studied for DNP are summarized in Table 2.

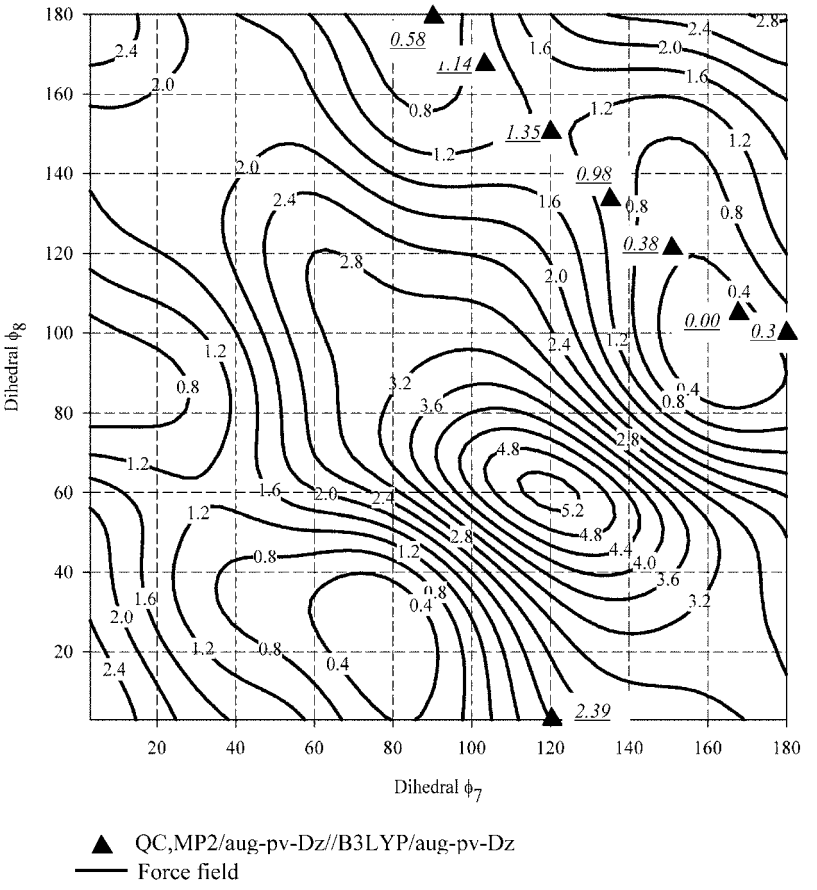

Figure 3. Comparison of conformational energies for DNP obtained from force field to quantum chemistry results (dihedral angles in degrees, relative energies in kcal/mol; see Figure 1(e); additional details in Table 3).

The torsional parameters for O−N−C−C were transferred from DNP to DNMP. Using the charges from Table 6 (DNP), the torsional parameters for C−C−C−O, C−C−O−C, and N−C−C−O (Figure 1(d)) were adjusted to match molecular mechanics and quantum chemistry energies and geometries. The conformational energy path for the C−C−C−O torsion is

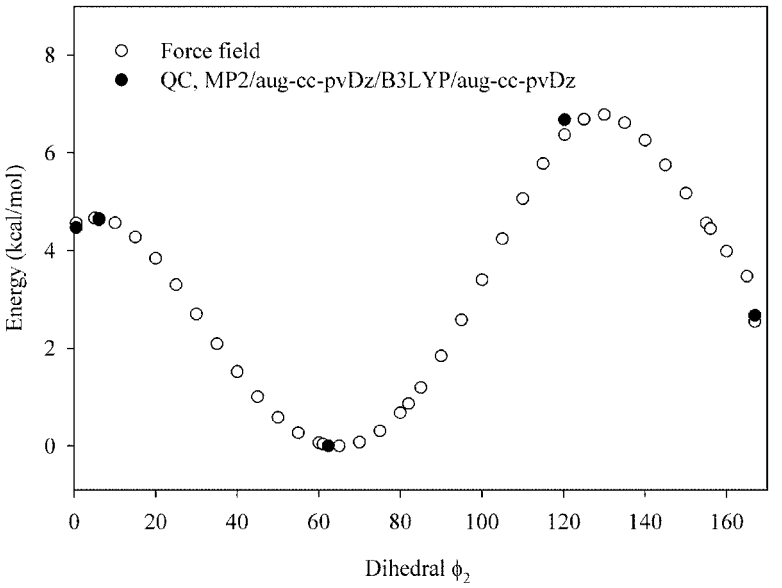

Figure 4. Comparison of conformational energies for DNMP calculated from the force field to quantum chemistry results at the MP2/aug-cc-pvDz//B3LYP/aug-cc-pvDz level of theory (dihedral angle in degrees, relative energies in kcal/mol).

shown in Figure 4. The minimum energy C−C−C−O (φ_1, φ_2) conformation at the MP2/aug-cc-pvDz//B3LYP/aug-cc-pvDz level was found to be *gt* (62.3°, 172.3°). Comparisons of the energies of all the conformations studied for DNMP, including a large number of conformations with one or both torsions fixed, are summarized in Table 3. The out-of-plane bend force constants for O−N−O−C were taken to be equal to the O−N−O−N out-of-plane bend force constants in HMX [3].

Transferability of the Force Field from Model Compounds to BDNPF

As a part of our validation of the potential, we studied the transferability of the force field parameters developed for

model compounds to BDNPF. We performed quantum chemistry studies on BDNPF for five important geometric minima listed in Table 8, at the B3LYP/aug-cc-pvDz level. (In this case MP2/aug-cc-pvDz//B3LYP/aug-cc-pvDz was not computationally tractable with the available resources.) The *gtggtg* conformer was found to have the minimum energy. The comparison between quantum chemistry– and molecular mechanics–based force field energies and the geometries reveals that the developed potential can be successfully transferred to BDNPF. The deviation between the quantum chemistry– and molecular mechanics–based energy differences is less than 0.25 kcal/mol for all geometries. The deviation in torsional angles between quantum chemistry– and molecular

Table 8
Comparison between the conformational energies and backbone torsions for bis(2,2-dinitropropyl)formal (BDNPF) calculated using the force field (normal text) and quantum chemistry (B3LYP/aug-cc-pvDz, italics)

Conformer	Energy (kcal/mol)	Torsion (degree)					
		$\boldsymbol{\varphi_1}$[a]	$\boldsymbol{\varphi_2}$	$\boldsymbol{\varphi_3}$	$\boldsymbol{\varphi_4}$	$\boldsymbol{\varphi_5}$	$\boldsymbol{\varphi_6}$
gtggtg	0.00	65.3	184.8	82.1	82.1	184.8	65.3
	0.00	*61.8*	*184.6*	*61.3*	*59.4*	*182.4*	*65.7*
gtgttg	1.78	66.9	187.8	82.2	179.1	174.6	66.0
	1.89	*64.2*	*168.7*	*71.3*	*184.6*	*174.8*	*64.1*
gttttg	4.82	64.4	172.2	177.3	177.3	172.7	64.4
	5.03	*62.0*	*173.6*	*171.4*	*171.4*	*173.6*	*62.2*
ttggtg	2.12	173.6	203.8	80.5	81.0	192.0	66.9
	2.11	*168.1*	*194.6*	*71.8*	*72.6*	*176.5*	*65.5*
ttggtt	2.84	170.4	185.1	70.5	70.5	185.1	170.4
	2.59	*192.1*	*179.4*	*62.8*	*62.6*	*179.5*	*192.5*

[a] $\boldsymbol{\varphi_1}$ and $\boldsymbol{\varphi_6}$ represent C−C−C−O torsions, $\boldsymbol{\varphi_3}$ and $\boldsymbol{\varphi_4}$ represent C−O−C−O torsions, and $\boldsymbol{\varphi_2}$ and $\boldsymbol{\varphi_5}$ represent C−O−C−C torsions (see Figure 1(a)).

mechanics–based predictions is less than 20° for most of the geometries considered.

Extension of Force Field for BDNPF to BDNPA

For the simulations of a eutectic mixture of BDNPF and BDNPA, the force field developed for BDNPF was adapted to accommodate BDNPA. The repulsion/dispersion parameters developed for BDNPF were transferred directly to BDNPA without modification, and likewise for the bond, bend, torsion, and out-of-plane bends force constants. The charge on the carbon in the acetal group in BDNPA was adjusted such that the ''acetal'' group has a total charge equal to that of the ''formal'' hydrogen atom in BDNPF (referred to as H_l in Figure 2). The rest of the charges in BDNPA were taken to be equal to the corresponding charges in BDNPF. The bond, bend, torsion, and deformation force constants for BDNPA were taken from the corresponding force constants developed in the force field for BDNPF. For the H−C−C−O and H−C−C−H torsions, which are not present in BDNPF, the torsional parameters were taken from the force field on poly (ethylene oxide) [11].

4. Molecular Dynamics Simulations

Molecular Dynamics Methodology

All simulations were carried out using the *lucretius* MD simulation package [19], using the Nose-Hoover thermostat and barostat. All production runs correspond to a pressure of one atmosphere. A cutoff radius of 10 Å was used for all van der waals interactions. A multiple time-step integrator described elsewhere [20] was employed. Covalent bond lengths were constrained using the SHAKE algorithm [21]. The time step of integration for high-frequency vibrations (bends and torsions) was 0.5 fs. Nonbonded interactions within a cutoff radius of 6 Å were evaluated every 1.0 fs, and those between 6 Å and 10 Å were evaluated every 2.0 fs. To account for long-range electrostatic interactions, the particle Mesh Ewald algorithm [22]

was used. The atomic stress tensor (employed in shear viscosity calculations described below) was recorded every 10.0 fs. Further details regarding simulations specific to particular systems and properties are provided in Table 4. For calculation of density and enthalpy of vaporization, equilibration was performed for at least five times as long as the slowest relaxation time in a given system (referred to as the Rouse time in Table 4 and defined as the time at which backbone end-to-end autocorrelation function decayed to a value of e^{-1}). To calculate the steady shear viscosity, equilibration was performed for at least 20 times the longest relaxation time of the system, and the production run time was at least 300 times that relaxation time.

Thermodynamic Properties

We investigated the ability of our force field to reproduce/predict a variety of thermodynamic and transport properties of liquid dinitro compounds, including liquid DNE, DNP, and BDNPF/A eutectic.

Atomistic simulations were performed for DNE and DNP at 298 K in the isobaric-isothermal (NPT) ensemble, in a cubic, three-dimensionally periodic simulation cell. The density and enthalpy of vaporization of DNE obtained from our liquid phase molecular dynamics simulations are 2.8(±0.5)% and 2.7(±0.3)% lower than the respective experimental values [23,24] (see Table 4). In the case of DNP, the density from simulations at 298 K is 2.5(±0.3)% lower than experiment [25], and the enthalpy of vaporization is 1.0(±0.5)% higher than the reported value [23] (see Table 4). Overall, the calculated densities and enthalpies of vaporization of DNE and DNP are in close agreement with experimental values.

The enthalpy of vaporization of BDNPF at 400 K was obtained based on isothermal-isochoric (NVT) MD simulations in a cubic box (see Table 4); the force field predicts a value of 22.6(±0.1) kcal/mol for this quantity. However, no direct experimental measurements of the enthalpy of vaporization for BDNPF are available in the literature. Hence an approximate value was estimated by reading the vapor-pressure (P) curve

for BDNPF [26] and using the Clausius-Clapeyron equation to obtain the enthalpy of vaporization (ΔE_{vap}):

$$\frac{d \ln P}{dT} = \frac{\Delta E_{vap}}{RT^2}, \tag{8}$$

where R is the universal gas constant and T is the absolute temperature. The approximate value thus obtained for the enthalpy of vaporization of BDNPF at 400 K is 17.9($\pm$0.4) kcal/mol.

Molecular dynamics simulations were performed on a mixture of 32 molecules of BDNPF and 30 molecules of BDNPA (i.e., the 50/50-wt% eutectic that comprises BDNPF/A plasticizer) to obtain an equilibrium density for the mixture. The eutectic mixture was allowed to relax initially at lower densities, after which the density of the system was gradually increased to the experimental value. After that the system was equilibrated using NPT-MD at 298 K, until a steady-fluctuating density was achieved. The resulting value was 1.359 ($\pm$0.015) g/cc, which is in excellent agreement (1.7–2.7% lower) with the experimental value of 1.383–1.397 g/cc [26].

Isothermal-isobaric MD simulations of the BDNPF/A eutectic mixture were also performed at 328 K to obtain the speed of sound in the melt. At constant temperature and pressure, the isothermal bulk modulus (β_T) is related to volume fluctuations by [27]

$$\beta_T = VK_BT/\langle \delta V^2 \rangle_{NPT}, \tag{9}$$

where K_B is Boltzmann constant and V is the average volume of the system at temperature T. From this, the speed of sound C can be obtained using

$$C = \sqrt{\frac{\beta_T}{\rho}}, \tag{10}$$

where ρ is the average density of the system.

Experimentalists have used impulsive stimulated light scattering (ISLS) to measure the sound speed in BDNPF/A eutectic

at 328 K, and obtained a value of 1297.4–1301.9 m/s [26]. The sound speed from our simulations is found to be 1323 (± 4) m/s, which is in quite reasonable agreement with the experiments. (We note that, since it is an isentropic measurement, the ISLS sound speed should be greater than the corresponding isothermal value by perhaps a few percent, but we nevertheless regard the level of agreement obtained as a successful validation point for the force field.)

Transport Properties

The apparent self-diffusion coefficient for DNP from MD simulations at 357 K is 0.70×10^{-9} ($\pm 0.03 \times 10^{-9}$) $m^2 s^{-1}$ which is about 30% less than the experimental value of $1.0 \times 10^{-9} m^2\ s^{-1}$ [28] (Figure 5). At 345 K it is $0.50 \times 10^{-9} (\pm 0.02 \times 10^{-9})$ $m^2 s^{-1}$, compared to $0.89 \times 10^{-9} m^2 s^{-1}$ from experiment [28].

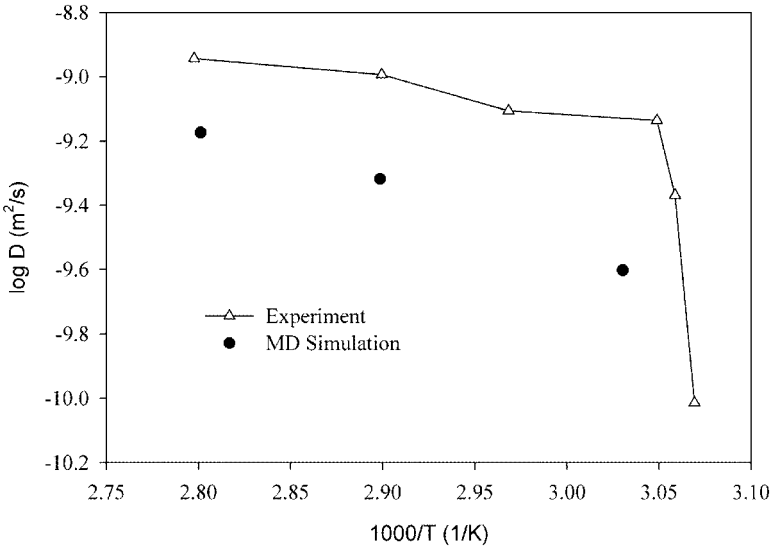

Figure 5. Comparison of the self-diffusion coefficient for DNP obtained from MD simulations using the force field developed in this work to experimental results. (Calculated error bars were smaller than the symbol size and hence not included in the plot.)

Zero-frequency shear viscosities of the BDNPF/A eutectic were calculated in the temperature interval 450–700 K, in 50 K increments, using the Einstein relation [27]

$$\eta = \lim_{t\to\infty} \frac{V}{6K_B Tt} \left(\left\langle \sum_{\alpha\neq\beta} (L_{\alpha\beta}(t) - L_{\alpha\beta}(0))^2 \right\rangle \right), \qquad (11)$$

where $L_{\alpha\beta}(t) = \int_0^t P_{\alpha\beta}(t')dt'$, K_B is the Boltzmann constant, T is temperature, t is time, $P_{\alpha\beta}$ is the symmetric stress sensor, and V is the fixed volume of the simulation box. The lengths of simulation trajectories were chosen such that $t_{sim} >> \tau_\eta$, where τ_η is the viscosity relaxation time defined as

$$\eta(\tau_\eta) = (1 - e^{-1})\eta(t_{sim} \to \infty). \qquad (12)$$

The shear viscosity was calculated by averaging the apparent viscosity data obtained from the Einstein equation for the specified time interval. The details of the methodology used to estimate the apparent average shear viscosity can be found in our previous work on HMX [29]. Even with this approach, we could not compare directly our calculated shear viscosity to experimental values, which were measured in the vicinity of room temperature, since the required simulation lengths would have been impractical. Therefore, we used temperature extrapolation to obtain the shear viscosity of the BDNPF/A eutectic at 323 K and at atmospheric pressure.

The measured and calculated results for the BDNPF/A shear viscosity are shown in Figure 6, along with the temperature extrapolation. The experimental value of the shear viscosity at 323 K is reported to be 59 cP [26]; our extrapolated prediction to that temperature is 62 cP. The calculated apparent activation energies are 5.6 and 6.7 kcal/mol for shear viscosity and self diffusion, respectively, in the temperature interval 450–700 K. The activation energy for shear viscosity extracted from the experimental data [26] in the temperature interval 280–323 K is 10.2 kcal/mol. According to the Eyring expression for dense fluids [30], the simple relation ($\Delta E_{vap} = n\Delta E_{vis}$, where $2 \leq n \leq 5$) holds for more than 100 substances, including associated liquids. The energy of vaporization is

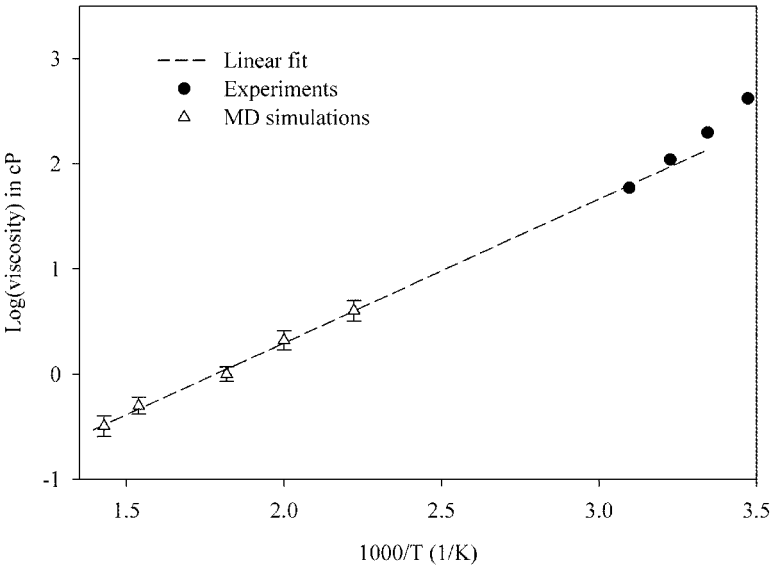

Figure 6. "Arrhenius plot" for zero-frequency shear viscosity of BDNPF/A plasticizer.

approximately equal to the cohesive energy; hence, it is possible to compare ΔE_{vap} and ΔE_{vis} determined directly from atomistic simulations. We obtain $\Delta E_{vap} = 22.3$ kcal/mol at 450 K, yielding a ratio $\Delta E_{vap}/\Delta E_{vis} = 3.9$, which is entirely consistent with the Eyring correlation.

5. Conclusions

We have developed a complete bonded and nonbonded force field for a series of energetic dinitro compounds representative of bis(2,2-dinitropropyl)formal/acetal (BDNPF/A) based upon extensive *ab initio* electronic structure calculations of geometries and energies. This potential was successfully used for atomistic simulations of 2,2-dinitropropane (DNP), 1,1-dinitroethane (DNE), and BDNPF/A. The densities for DNE and DNP obtained from MD simulations match experimental values to within 3%, whereas the enthalpies of vaporization

were within 7% of experimental values at 298 K and atmospheric pressure. The force field also reproduced the speed of sound in BDNPF/A to within a few percent. Predictions of transport behavior (self-diffusion coefficients for DNP and zero-frequency shear viscosities for BDNPF/A) were consistent with experiment. Based on these validation studies, we think the force field can be used with reasonable confidence for simulations of a variety of dinitro compounds. Further, at this point force-field development has been completed for all important constituents of the plastic-bonded explosive PBX-9501, thus enabling detailed investigations into the physico-chemical interactions that occur in that material.

Acknowledgments

This research is funded by the University of Utah Center for the Simulation of Accidental Fires and Explosions (C-SAFE), funded by Department of Energy, Lawrence Livermore National Laboratory, under Subcontract B341493. T.D.S. is funded by Los Alamos, which is supported by the United States Department of Energy under contract number W-7405-ENG-36 with the University of California. T.D.S. wishes to thank Richard Browning (Los Alamos) for useful discussions; and Bob Sander, Dana Dattelbaum, and Mike Whitehead (Los Alamos) for permission to use their ISLS-based sound speeds in the present article.

References

[1] "Stability of dinitro compounds," http://www.crhf.org.uk/incident82.html
[2] Gibbs, T. R. and A. Popolato. 1980. *LASL Explosive Property Data*, University of California, Berkeley, p. 109.
[3] Smith, G. D. and R. K. Bharadwaj. 1999. *J. Phys. Chem. B*, 103: 3570.
[4] Smith, G. D., D. Bedrov, O. G. Byutner, O. Borodin, C. Ayyagari, and T. Sewell. 2003. *J. Phys. Chem. A*, 107: 7552.
[5] Akhavan, J. 1998. *Polymer*, 39: 215.

[6] "Nitroplasticizer," http://www.dtcs-hycat.com/DoD Technology Chemicals.html
[7] Espada, L. I., J. T. Mang, B. Orler, D. A. Wrobleski, D. A. Langlois, and R. P. Hjelm. 2001. *Polymer Preprints*, 42: 693.
[8] Gore, G. M., R. G. Bhatewara, K. R. Tipare, N. M. Walunj, and V. K. Bhat. 2002. *J. Energ. Materials*, 20: 255.
[9] Frisch, M. J., G. W. Trucks, H. B. Schlegel, G. E. Scuseria, M. A. Robb, J. R. Cheeseman, V. G. Zakrzewski, et al. 1998. *Gaussian 98* revision A.7. Pittsburgh: Gaussian Inc.
[10] Becke, A. D. 1993. *J. Chem. Phys.*, 98: 5648.
[11] Lee, C., W. Yang, and R. G. Parr. 1988. *Phys. Rev. B*, 37: 785.
[12] Borodin, O. and Smith, G. D. 2004. In L. Curtiss and M. Gordon (eds.), *Methods and Applications in Computational Materials Chemistry*, Dordrecht: Kluwer, pp. 35–90.
[13] Smith, G. D. and Borodin, O. 2005. In V. Galiatsatos (ed.), *Molecular Simulation Methods for Predicting Polymer Properties*, New York: John Wiley & Sons, p. 45.
[14] Woon, D. E. and T. H. Dunning. 1994. *J. Chem. Phys.*, 100: 2975.
[15] Sorensen, R. A., W. B. Liau, L. Kesner, and R. H. Boyd. 1988. *Macromolecules*, 21: 200.
[16] Cornell, W. D., P. Cieplak, C. I. Bayly, I. R. Gould, K. M. Merz, D. M. Ferguson, D. C. Spellmeyer, T. Fox, J. W. Caldwell, and P. A. Kollman. 1995. *J. Am. Chem. Soc.*, 117: 5179.
[17] Bayly, C., P. Cieplak, W. Cornell, and P. A. Kollman. 1993. *J. Phys. Chem.*, 97: 10269.
[18] Smith, G. D., R. L. Jaffe, and D. Y. Yoon. 1993. *J. Phys. Chem.*, 97: 12752.
[19] Ayyagari, C., G. D. Smith, D. Bedrov, and O. Borodin. 2004. "Lucretius," http://lucretius.mse.utah.edu
[20] Martyna, G. J., M. E. Tuckerman, D. J. Tobias, and M. L. Klein. 1996. *Molecular Phys.*, 87: 1117.
[21] Ryckaert, J., G. Ciccotti, and H. J. C. Berendsen. 1977. *J. Comput. Phys.*, 23: 327.
[22] Darden, T., D. York, and L. Pedersen. 1993. *J. Chem. Phys.*, 98: 10089.
[23] Piacenza, G., G. Jacob, H. Graindorge, B. Blaive, and R. Gallo. 1997. *28th International Annual Conference of ICT*, 123: 1.
[24] Miroshnichenko, E. A. and V. P. Vorobyeva. 1999. *Russian Journal of Physical Chemistry (Zhurnal Fizicheskoi Khimi)*, 73: 419.

[25] "Rocket Engine Specific Impulse Program," http://www.dunn-space.com/isp.htm
[26] Private communications to T. D. Sewell. Sound speed results: Dana M. Dattelbaum; all others: Ken Laintz.
[27] Allen, M. P. and T. J. Tildesley. 1987. *Fluctuations: Computer Simulations of Liquids*. Oxford: Oxford University Press.
[28] Grochulski, T. and L. Pszczólkowski. 1992. *Phys. Rev. Lett.*, 68: 3635.
[29] Bedrov, D., G. D. Smith, and T. D. Sewell. 2000. *J. Chem. Phys.*, 112: 7203.
[30] Glasstone, S., K. J. Laidler, and H. Eyring. 1941. *The Theory of Rate Processes*. New York: McGraw-Hill.